

# Hadronic Structure Functions<sup>1</sup>

Martin Erdmann

Institut für Experimentelle Kernphysik, Universität Karlsruhe,  
Engesserstr. 7, D-76128 Karlsruhe, Martin.Erdmann@desy.de

## Abstract

Experimental results on hadronic structures are discussed in view of our physics understanding. Achievements and challenges are noted.

---

<sup>1</sup>Invited opening plenary talk at the 8th International Workshop on Deep Inelastic Scattering and QCD, Liverpool, UK (2000)

# 1 Motivation

Today's motivation of measuring lepton–hadron scattering processes is at least four-fold. Fig.1 shows basic diagrams at electron–positron, hadron–hadron, and lepton–hadron colliders:

- Only in lepton–hadron collisions is the fusion diagram forbidden within the Standard Model, which strongly motivates **searches for new physics**, e.g. leptoquarks.

The exchange of bosons allows different hadronic structures to be probed:

- The prototype for **existing hadronic structures** is the proton which currently is the most precisely studied hadronic object.
- **Genesis of hadronic structures** is analysed using the structure developing in quantum fluctuations of the photon.
- **Colour singlet exchange** constitutes a process beyond single boson exchange. It's successful description provides a prime challenge for QCD.

It is the purpose of this contribution to underline these different aspects of lepton-hadron scattering physics and their perspectives using as much as possible the measurements themselves.

LEP/TESLA

TEV/LHC

HERA  
LEP/TESLA

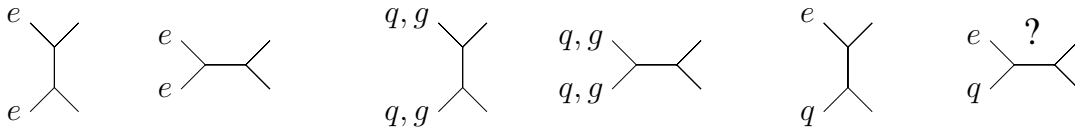


Figure 1: Basic diagrams at electron–positron, hadron–hadron, and lepton–hadron colliders. Only the last diagram is forbidden within the Standard Model.

## 2 Lepton–Quark Scattering at Attometer Distance

The large center of mass energy at HERA of  $\sqrt{s_{ep}} = 318$  GeV allows lepton–quark scattering to be analysed at distances down to almost 1 Attometer =  $10^{-18}$  m. Both neutral and charged current interactions (Fig.2) are used to test the Standard Model predictions. The double differential cross sections in terms of the resolution scale  $Q^2$ , which denotes the negative squared

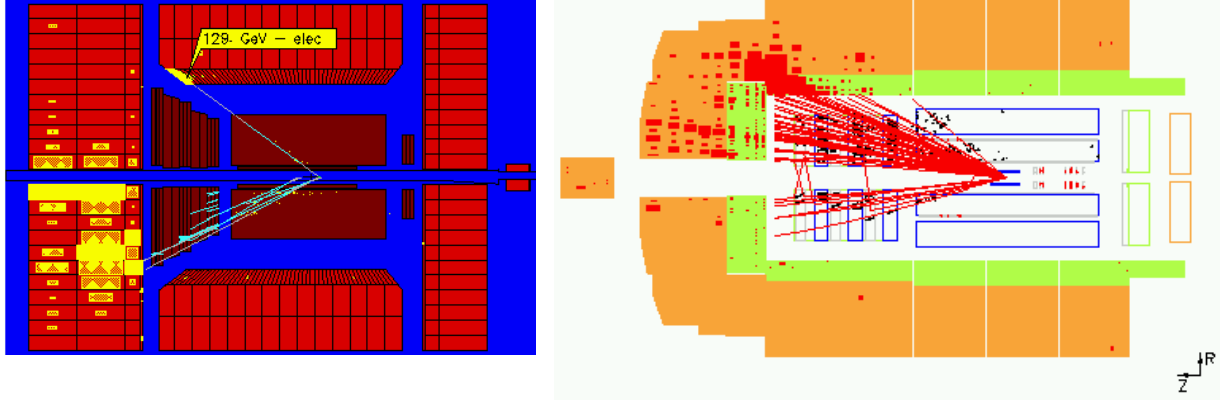


Figure 2: Neutral and charged current interactions observed with the ZEUS and H1 experiments.

four-momentum transfer carried by the boson, and the quark fractional momentum  $x$  relative to the proton are given by:

$$\frac{d^2\sigma_{NC}}{dQ^2 dx} \sim \alpha^2 \frac{1}{Q^4} \frac{1}{x} \Phi_{NC}(x, Q^2) \quad (1)$$

$$\frac{d^2\sigma_{CC}}{dQ^2 dx} \sim G_F^2 \left( \frac{M_W^2}{M_W^2 + Q^2} \right)^2 \frac{1}{x} \Phi_{CC}(x, Q^2) \quad (2)$$

Here  $\alpha$  and  $G_F$  denote the coupling strength of the electromagnetic and weak interaction processes.  $M_W$  is the  $W$ -boson mass. The  $\Phi$  terms denote the spin characteristics of the scattering together with the probabilities  $xf(x, Q^2)$  of finding the different quark flavours in the proton. In addition  $\Phi_{NC}$  contains terms for  $Z$  exchange and  $\gamma$ - $Z$  interference. At high  $Q^2$  it is

$$\Phi_{NC}^{e^\mp p} \sim \left( 1 + \cos^4 \left( \frac{\theta^*}{2} \right) \right) \left( \frac{4}{9}(xu + x\bar{u}) + \frac{1}{9}(xd + x\bar{d}) \right) \pm \text{add. terms with } \gamma, Z \quad (3)$$

$$\Phi_{CC}^{e^- p} \sim xu + \cos^4 \left( \frac{\theta^*}{2} \right) x\bar{d} \quad (4)$$

$$\Phi_{CC}^{e^+ p} \sim x\bar{u} + \cos^4 \left( \frac{\theta^*}{2} \right) xd \quad (5)$$

$\theta^*$  denotes the scattering angle in the lepton-quark center of mass system and can be calculated from  $\cos^4(\theta^*/2) = (1 - Q^2/s_{ep}/x)^2$ . The two components in the angular distribution result from two spin configurations of the colliding lepton and quark: if the spins add up to zero, any scattering angle is allowed. If the spins add up to 1, backward scattering is forbidden for massless quarks and the angular distribution is weighted by  $\cos^4(\theta^*/2)$ . In charged current interactions also the quark type can be analysed: e.g., positrons couple only to negatively charged quarks. In addition, right-handed positrons couple only to right-handed antiquarks, or left-handed quarks. This offers a unique handle to differentiate between quark flavours in the proton.

**Figure 1** shows the differential cross-section  $\frac{d\sigma}{dQ^2}$  in pb GeV $^{-2}$  as a function of the squared four-momentum transfer  $Q^2$  in GeV $^2$ . The plot is on a log-log scale. The y-axis ranges from  $10^{-7}$  to  $10^1$ , and the x-axis ranges from  $10^2$  to  $10^5$ . The data points are from H1 (red circles) and ZEUS (red squares) for Neutral Current (NC) and Charged Current (CC) processes. The Standard Model is shown as a solid red line for NC and a solid blue line for CC. The y-axis is labeled  $\frac{d\sigma}{dQ^2} / \text{pb GeV}^{-2}$  and the x-axis is labeled  $Q^2 [\text{GeV}^2]$ . The legend indicates:  $e^-p$  preliminary, Neutral Current (red), Charged Current (blue), H1 ( $y < 0.9$ ) (red circles), ZEUS (red squares), Standard Model (red line), H1 ( $y < 0.9$ ) (blue triangles), ZEUS (blue inverted triangles), and Standard Model (blue line). Two Feynman diagrams are shown on the right: the top one for NC (γ, Z exchange) and the bottom one for CC (W exchange).

Integrating the double differential cross sections over  $x$  gives the single differential cross section which is shown in Fig.3 as a function of  $Q^2$  from H1 [1] and ZEUS [2] data. Around  $Q^2 \sim 10^4 \text{ GeV}^2$  the cross sections are found to be of equal magnitude. Since in both neutral current and charged current electron-proton scattering at high  $Q^2$  primarily the  $u$ -valence quarks are probed, eqs. (3, 4), these data establish direct observation of the unification of the neutral current and charged current interactions at a resolution scale corresponding to about 10 Attometer.

Also in neutral current interactions, the data are over a wide range compatible with a linear rise: they reflect two equally large components, explained by the two spin configurations of the electromagnetic processes, eq. (3). The forward scattering region ( $\cos^4(\theta^*/2) = 1$ ) shows

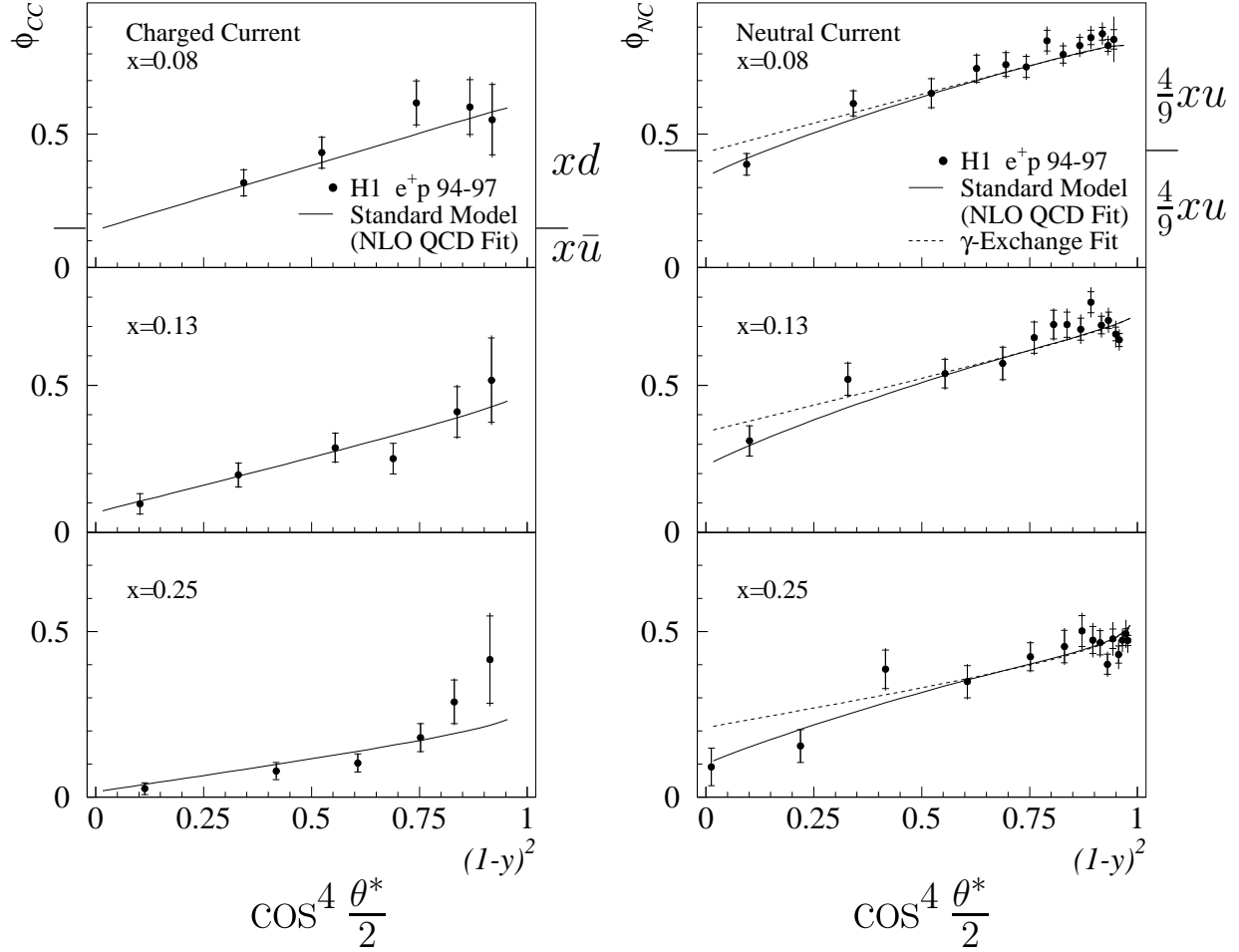


Figure 4: H1 measurements of the double differential charged and neutral current positron-proton cross sections as a function of  $\cos^4(\theta^*/2)$  in different bins of the parton fractional momentum  $x$ .  $\theta^*$  denotes the scattering angle in the lepton-quark center of mass system.

approximately the  $u$ -quark density in the proton:  $2 \times 4/9 xu \sim xu$ . In the region of backward scattering processes ( $\cos^4(\theta^*/2) = 0$ ), the cross section measurements deviate from the linear rise and demonstrate the onset of a new interaction: the lower cross section results from the negative interference between the photon and the  $Z$ -boson.

The comparison of the positron-proton neutral current and charged current data in the forward scattering region of Fig.4 demonstrates directly from the data that the  $u$ -quark density is twice that of the  $d$ -quark. Therefore the proton consists of the  $uud$  quark configuration also at the small distance scales probed at HERA.

The HERA luminosity upgrade program, starting to take data in 2001, is eagerly awaited: much more precise data will challenge the Standard Model predictions for  $ep$  processes in the Attometer regime.

### 3 Existing Hadronic Structure: Proton

As discussed in the previous section, the  $uud$  valence structure of the proton has been re-confirmed in the high  $Q^2$  neutral and charged current measurements at HERA. In the following our physics understanding of the proton structure function  $F_2$  is discussed.  $F_2$  is determined from measurements of the double differential neutral current cross section (compare with eqs. (1, 3))

$$\frac{d^2\sigma}{dQ^2 dx} \sim \alpha^2 \frac{1}{Q^4} \left( 1 + \cos^4 \left( \frac{\theta^*}{2} \right) \right) \frac{1}{x} F_2(x, Q^2) \quad (6)$$

and contains the individual quark distributions, weighted by the quark squared charges:

$$F_2(x, Q^2) \sim \frac{4}{9}(xu + x\bar{u}) + \frac{1}{9}(xd + x\bar{d}) + \frac{1}{9}(xs + x\bar{s}) + \dots \quad (7)$$

The QCD evolution equations predict that measurements of hadronic structures depend on the logarithm of the resolution scale  $Q^2$  at which the structure is probed. On this basis, the following ansatz to analyse the  $x$ -dependence of structure function data is explored [4]:

$$F_2(x, Q^2) = a(x) \left[ \ln \left( \frac{Q^2}{\Lambda^2} \right) \right]^{\kappa(x)}. \quad (8)$$

Here  $\Lambda$  is a scale parameter,  $a$  reflects the charge squared weighted quark distributions extrapolated to  $\ln(Q^2/\Lambda^2) = 1$ , and  $\kappa$  determines the positive and negative scaling violations of  $F_2$ .

In Fig.5, published ZEUS [5] low- $x$  data of the proton structure function  $F_2$  for  $Q^2 > 2$  GeV<sup>2</sup> are shown. In each  $x$ -bin, the result of a two-parameter fit according to eq. (8) is shown, using a fixed value of  $\Lambda = 0.35$  GeV which represents a typical value of the strong interaction scale. Only the total experimental errors have been used, ignoring correlations between individual data points. The same fitting procedure has been applied to BCDMS data [6] which are taken here as a reference sample for the high- $x$  region.

The resulting parameters  $a$  and  $\kappa$  are summarized in Fig.6 as a function of  $x$  together with fits to the published H1 low- $x$  data [7]. Also shown are fits to the preliminary H1 data [8] which are much more precise than the previous measurements.

For  $a$ , the data fits exhibit two distinct regions: around  $x \sim 0.3$  they reflect the valence quark distributions, implying that each valence quark carries  $\sim 1/3$  of the proton momentum. At low  $x$ ,  $a(x)$  is compatible with converging to a constant value. A comparison of the lowest point, derived from the H1 preliminary measurement, with the new ZEUS preliminary data presented at this conference will be of interest. The resulting scaling violation term  $\kappa$  appears to rise as  $x$  decreases, exhibiting the negative and positive scaling violations of  $F_2$  for  $x$  above and below 0.1 respectively. The errors in Fig.6 represent the statistical errors of the fits. Both parameters  $a$  and  $\kappa$  are anti-correlated as can be seen from neighbouring points. No significant  $Q^2$ -dependence of  $a$  and  $\kappa$  has been found in the published data when the fits were repeated for two intervals in  $Q^2$  (above and below 20 GeV<sup>2</sup>).

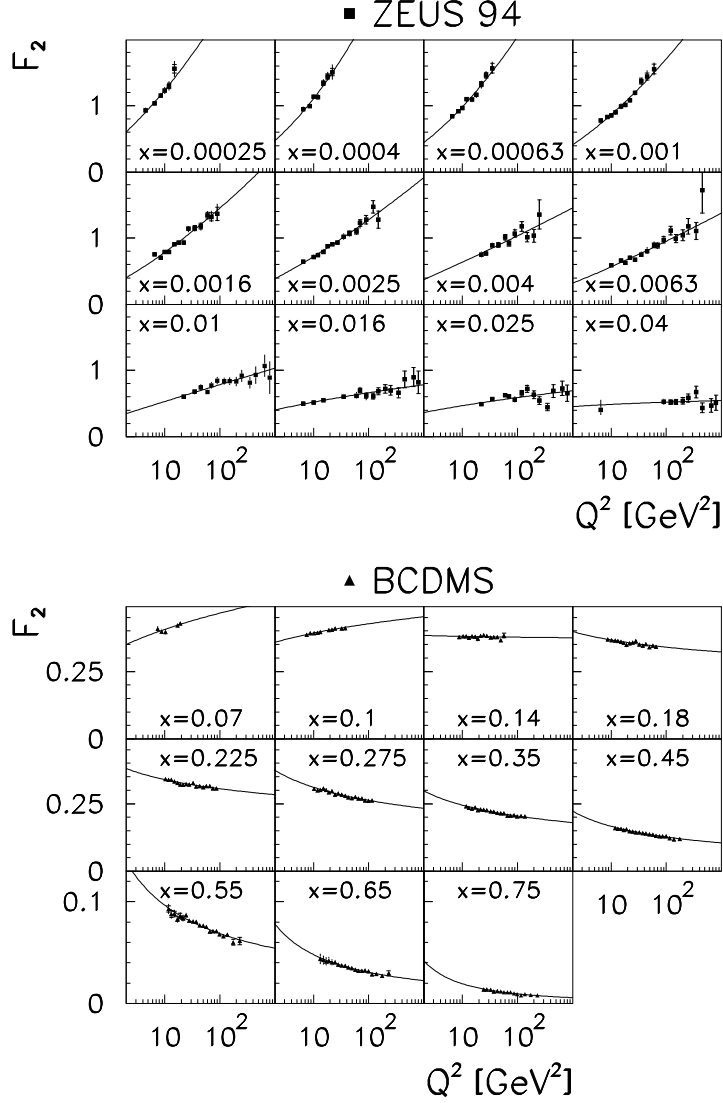


Figure 5: ZEUS and BCDMS measurements of the proton structure function  $F_2$  are shown as a function of  $Q^2$  in the range  $10^{-4} < x < 1$ . They are compared to the 2-parameter fits according to eq. (8) in each  $x$ -bin.

With  $a$  being approximately constant below  $x \sim 10^{-2}$ , changes of  $F_2$  at low  $x$  result from the scaling violation term  $\kappa$  alone, indicative of the interaction dynamics that drives  $F_2$  and in support of the predictions [9, 10].

The parameter  $a$  has already been identified as the charge squared weighted quark distributions extrapolated to  $\ln(Q^2/\Lambda^2) = 1$  which corresponds here to  $Q^2 = 0.3 \text{ GeV}^2$ . An understanding of the parameters  $\Lambda$  and  $\kappa$  can be achieved by comparison with the QCD evolution equation which is written here in the leading order DGLAP approximation:

$$\frac{df_i(x, Q^2)}{d \ln Q^2} = \frac{\alpha_s(Q^2)}{2\pi} \sum_j \int_x^1 \frac{dy}{y} P_{ij} \left( \frac{x}{y} \right) f_j(y, Q^2). \quad (9)$$

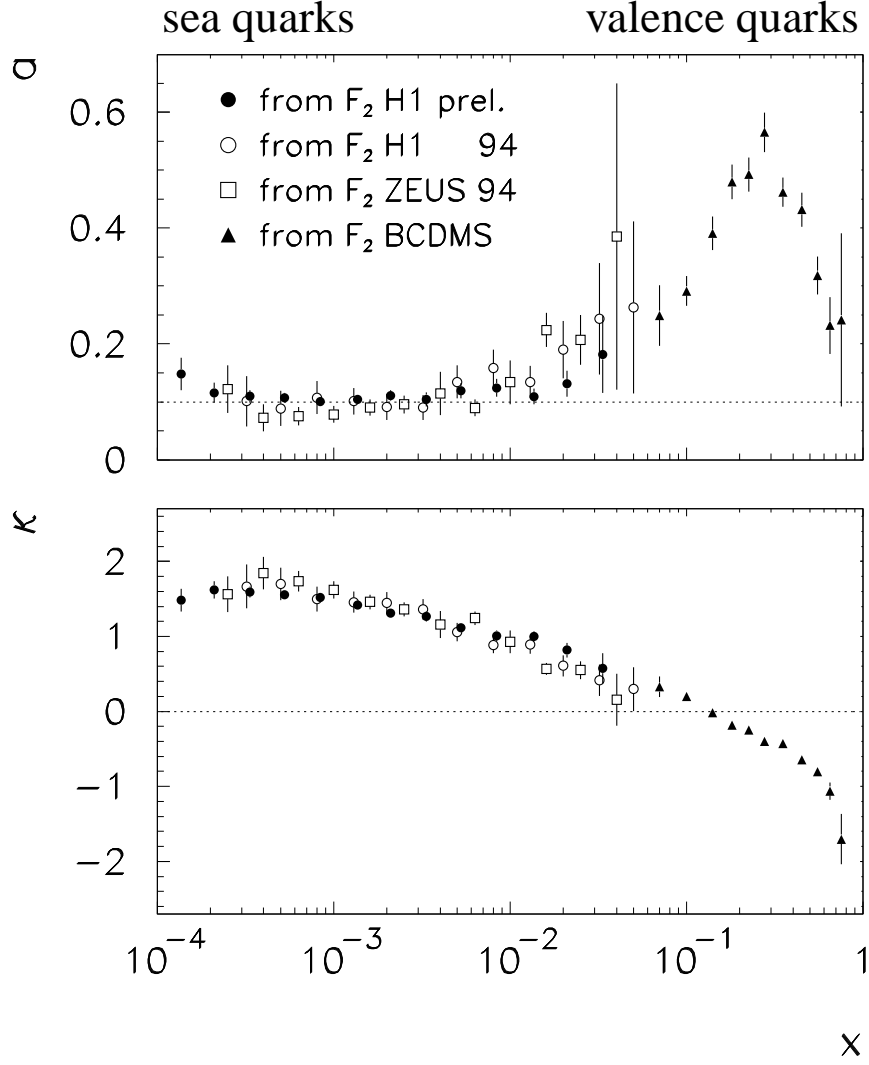


Figure 6: The quark distribution  $a(x)$  of the proton extrapolated to  $Q^2 = 0.3 \text{ GeV}^2$  and the scaling violations  $\kappa(x)$  from the fits to the published H1, ZEUS, BCDMS, and to the H1 preliminary data according to eq. (8). The dotted lines serve to guide the eye.

Here  $f_i, f_j$  denote the parton densities,  $P_{ij}$  are the splitting functions, and

$$\alpha_s = \frac{b}{\ln(Q^2/\Lambda_{QCD}^2)} \quad (10)$$

is the strong coupling constant.

The derivative of the ansatz chosen here, eq. (8), with respect to  $\ln Q^2$  gives

$$\frac{dF_2(x, Q^2)}{d \ln Q^2} = \frac{1}{\ln(Q^2/\Lambda^2)} \kappa(x) F_2(x, Q^2), \quad (11)$$

where relating  $1/\ln(Q^2/\Lambda^2)$  with  $\alpha_s$  in eq. (9) implies association of the scale parameter  $\Lambda$  in eq. (8) with the QCD parameter  $\Lambda_{QCD}$ . The term  $\kappa$  relates to the sum over the different parton radiation terms in eq. (9) divided by  $F_2$ .  $\kappa$  increases towards small  $x$ , consistent with larger phase space available for parton radiation.



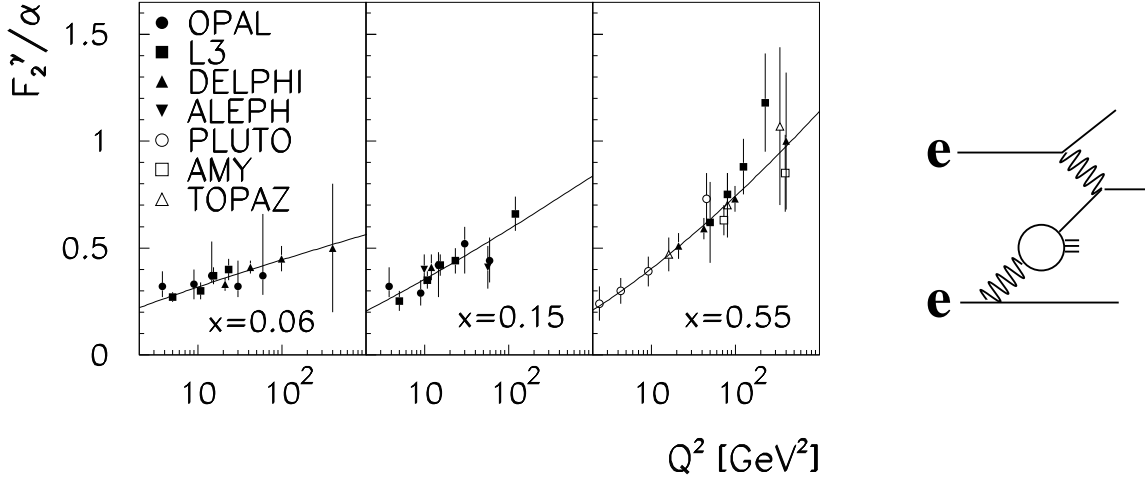


Figure 7: Measurements of the photon structure function are shown as a function of  $Q^2$ . They are compared to the 2-parameter fits according to eq. (8) in each  $x$ -bin.

To match the description chosen here, eq. (8), with the double asymptotic approximation expected from QCD for the gluon-dominated region at small  $x$ ,  $F_2 \sim \exp \sqrt{-\ln x \ln(\ln(Q^2/\Lambda^2))}$  [9, 11], the scaling violation term  $\kappa$  is required to have a dependence like

$$\kappa \sim \sqrt{\frac{-\ln x}{\ln(\ln(Q^2/\Lambda^2))}} \quad (12)$$

The  $Q^2$ -dependence of  $\kappa$  is therefore expected to be very small which is in agreement with the experimental observation stated above.

More precise data and data reaching smaller values of  $x$  will determine whether or not the scaling violations further increase towards low- $x$  and therefore give valuable information on the parton densities in the proton as  $x$  approaches 0.

## 4 Genesis of Hadronic Structure: Photon

The photon structure results from fluctuations of a photon into a colour neutral and flavour neutral hadronic state. For comparison with the proton data, the same fits according to eq. (8) have been applied to recent measurements of the photon structure function  $F_2^\gamma$  which have been performed at  $e^+e^-$  colliders [12] (Fig.7).

The values of the parameters  $a$  and  $\kappa$  are shown in Fig.8 as the open circles. Both parameters are distinct from those of a hadronic bound state like the proton: in  $a(x)$  the photon data exhibit no valence quark structure. Instead, in the low- $x$  region around  $x \sim 0.1$  the photon data prefer similar values of  $a$  to the proton data for  $x \leq 0.01$ . The scaling violations  $\kappa$  are positive at all values of  $x$  and  $\kappa$  is approximately 1. This is as expected from QCD calculations which predict  $F_2^\gamma$  for  $0.1 < x < 1$  [13].

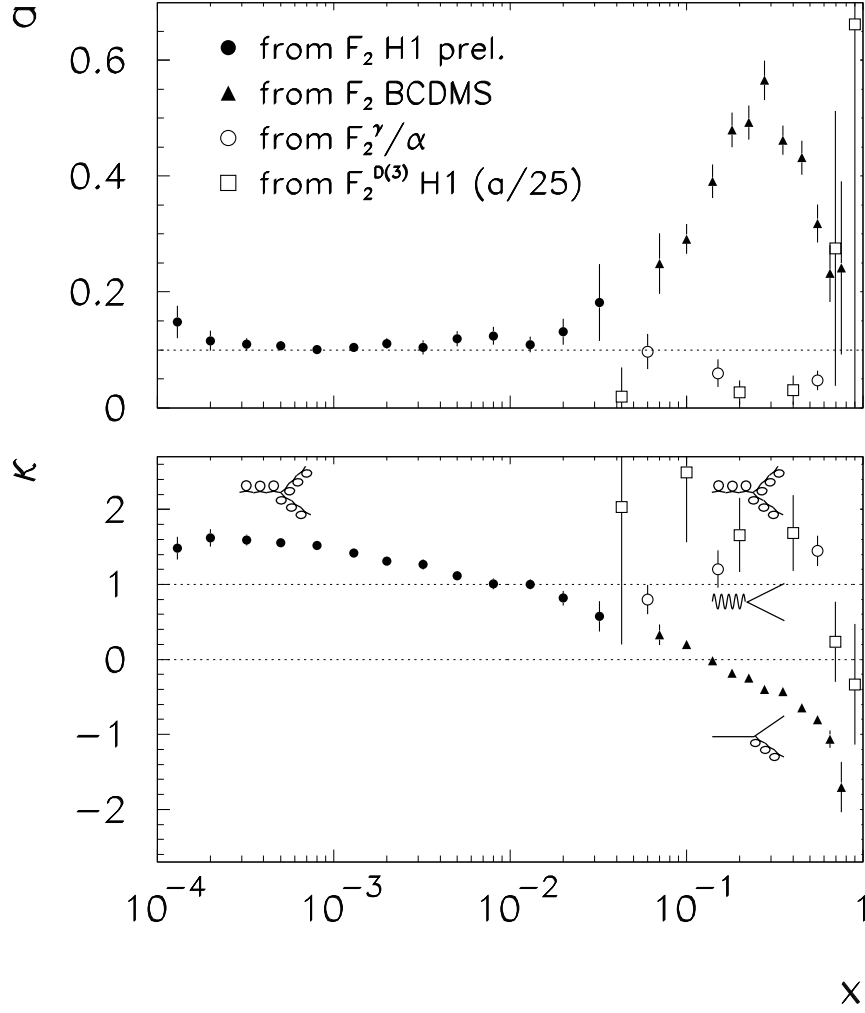


Figure 8: The hadronic structures  $a(x)$ , extrapolated to  $Q^2 = 0.3 \text{ GeV}^2$ , and the scaling violations  $\kappa(x)$  from fits to structure function data according to eq. (8) are compared between the proton, photon, and colour singlet exchange. The diagrams of splitting functions indicate regions they contribute to the QCD evolution. The lines serve to guide the eye.

Judgement on a universal low- $x$  behaviour of hadronic structures will result from more precise measurements and lower- $x$  data of the photon structure function. If the photon data show a constant quark density at small  $x$  similar to the low- $x$  proton data, scaling violations of  $F_2^\gamma$ , which deviate from those resulting from the photon splitting into quark-antiquark pairs and approach those observed for the proton, could become visible below or slightly above  $x = 10^{-2}$  where also for the proton data it is  $\kappa \sim 1$ .

Interesting information on the question of universality comes already from measurements of the gluon in the photon probed in strong interaction processes in photon-proton collisions. The production of two-jet events is sensitive to the gluons developing in photon fluctuations. In Fig.9, a recent measurement of  $xg(x)$  is shown [14]. The gluons appear as the low- $x$  companions of the newly built hadronic structure: at large  $x$  the gluon density is small; it rises towards small values of  $x$ .

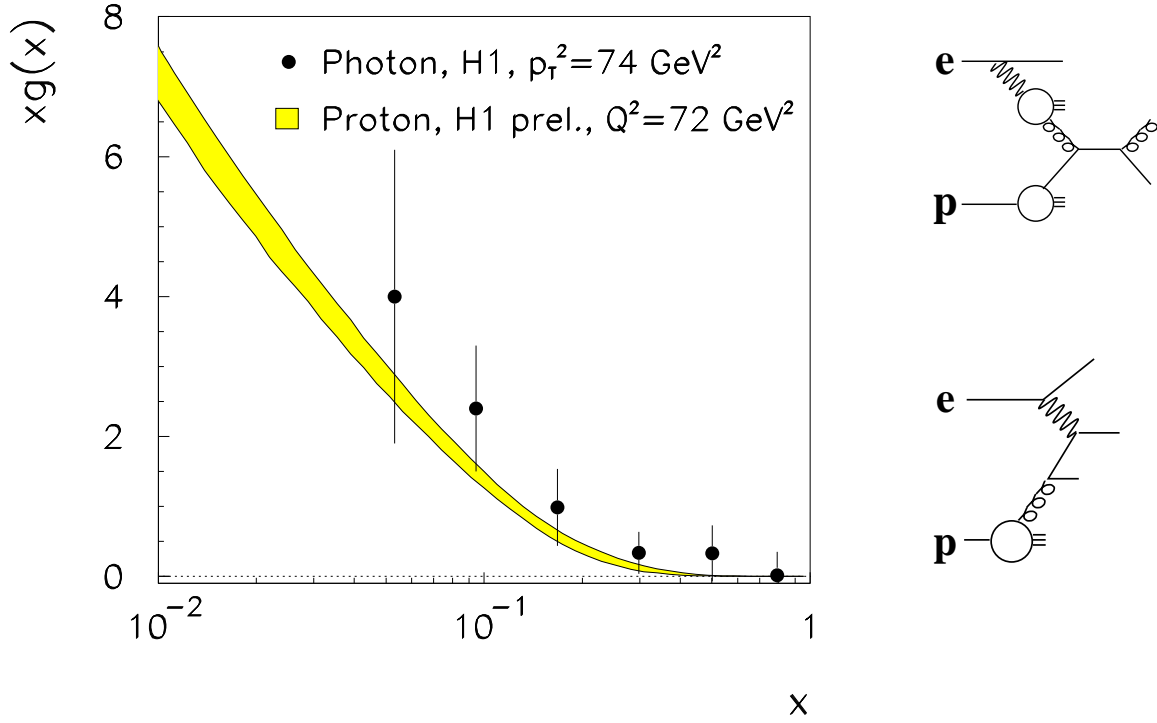


Figure 9: Comparison of the H1 photon and proton gluon distributions as a function of  $x$ .

In the same figure, this gluon distribution is compared to the gluon distribution of the proton, determined from measurements of the proton structure function [8]. Although the error bars of the photon measurement are large and  $Q^2$  and  $p_t^2$  may not represent the very same resolution scale, the similarity of the newly built and the already existing gluon distribution is striking. This observation may be a first experimental indication of a universal gluon distribution developing in hadronic structures.

## 5 Colour Singlet Exchange

Further information on gluons in hadronic structures results from structure function measurements of colour singlet exchange. In Fig.10, H1  $F_2^{D(3)}$  data [15] are compared to the same two-parameter fits as used above, eq. (8). Here  $x$  (frequently called  $\beta$ ) denotes the fractional momentum of the scattered parton relative to the colour neutral object, which itself carries a fractional momentum  $\xi = 0.003$  relative to the proton and therefore belongs to the low- $x$  companions of the proton.

Also these data exhibit scaling violations  $\kappa$  that are different from the proton measurements at the same values of  $x$  (Fig.8). Instead, for  $x < 0.5$  they have the tendency of being larger than the photon data and are similar to the low- $x$  proton data. The large rate of events with colour singlet exchange together with the large scaling violations of  $F_2^{D(3)}$  is suggestive of a gluon dominated exchange.

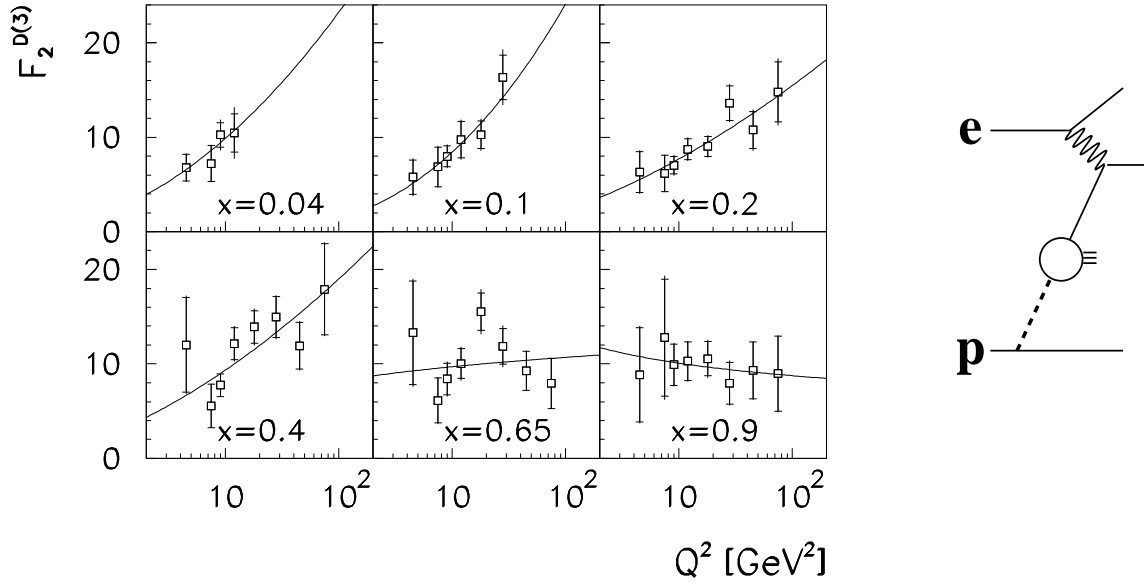


Figure 10: H1 measurements of the structure function of colour singlet exchange are shown as a function of  $Q^2$ . They are compared to the 2-parameter fits according to eq. (8) in each  $x$ -bin.

The values of the normalization  $a$  rise towards  $x = 1$  to about  $a = 10$  (in Fig. 8, the parameter  $a$  has been scaled by  $1/25$ ). These values have large uncertainties of the order of 100%. If more precise data support such a singular parton density for  $x \rightarrow 1$  at low  $Q^2$ , then these colour neutral fluctuations consist of one gluon carrying essentially all the colour singlet momentum and (at least) one further gluon with very low momentum neutralizing the colour.

## 6 Predictive Power for Proton Interaction Processes

The proton structure reveals amazing simplicity: at low resolution scale  $Q^2$ , the three valence quarks  $uud$  each carry fractional momentum  $x = 1/3$  (see sections 2, 3). The sea quark contribution is at low values of  $x$  independent of  $x$  (see section 3). Gluons accompany the proton at low  $x$  with a possibly universal momentum distribution (see section 4). Gluons initiate colour neutral configurations together with other very low momentum gluons (see section 5).

However, to predict interactions with protons, full information on all individual parton distributions of the proton are required. While such parton distribution functions  $xf_i$  have been available from global fits for many years, recent pioneering work has succeeded in determining the precision of these distribution functions taking into account the precision of the measurements and correlations between the different functions  $xf_i$  [16] (Fig.11). This analysis shows a good knowledge of the functions  $xf_i$  over a wide range in  $x$ . However, the knowledge for  $x \rightarrow 1$  is not satisfactory: large values of  $x$  correspond to high resolution power at hadron colliders (e.g. LHC) and point at the potential discovery region for new physics. An improved determination of the proton parton distribution as  $x$  approaches 1 by deep inelastic scattering experiments is therefore mandatory and currently is under discussion [17].

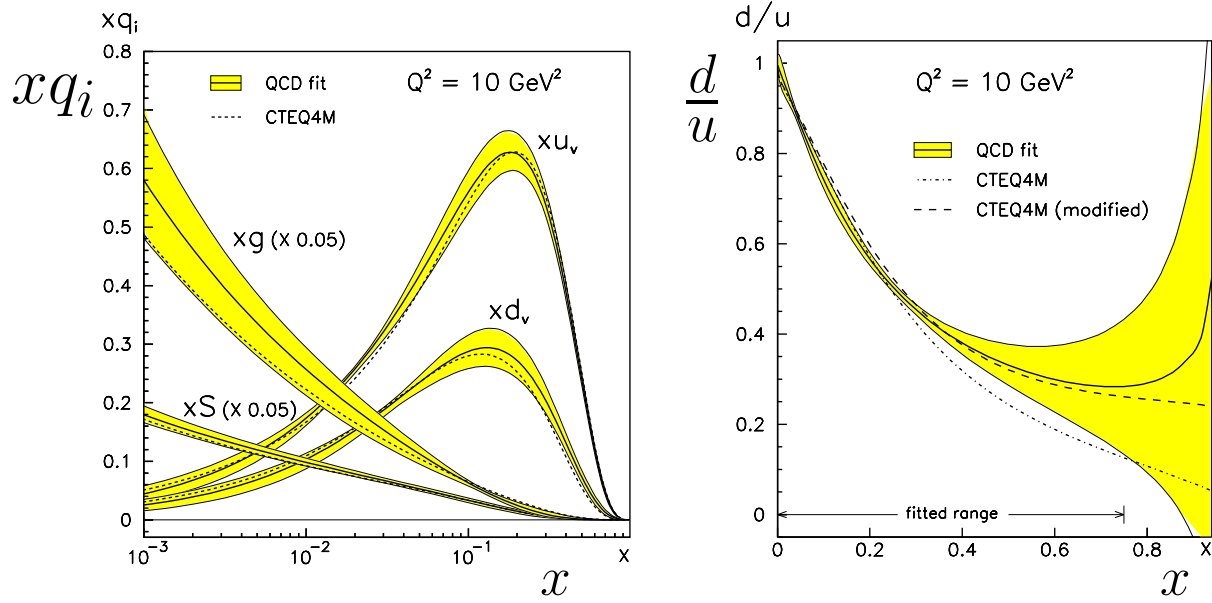


Figure 11: Parton distribution functions and  $d/u$  ratio as a function of  $x$  at  $Q^2 = 10 \text{ GeV}^2$  from a global fit which takes into account experimental errors and correlations between the individual parton distribution functions.

Further questions on the predictive power of QCD calculations for proton-proton interactions result from the measurements of forward jet and forward  $\pi^0$  cross sections in  $ep$  collisions, e.g. [18]. These measurements explicitly test QCD evolution over some rapidity distance and may signal limitations of the current approximations of QCD evolution to simple process configurations at small distances. Here theoretical work is needed and ongoing.

## 7 Achievements and Challenges

We currently celebrate the 30 years knowledge of valence quarks in the proton. The new contribution of the HERA collider experiments to the understanding of the proton is the low- $x$  structure which appears as a consequence of QCD dynamics. Open questions are: is the parton density of the proton finite as  $x \rightarrow 0$ ? What is the parton density at  $x \rightarrow 1$ ? Is the QCD evolution approximated correctly?

Measurements on the genesis process of hadronic structures use quantum fluctuations of the photon: since over 20 years we know the momentum distributions of quarks resulting from the photon splitting into quark-antiquark pairs. For the first time, the HERA and LEP experiments have measured the gluon distribution of newly built hadronic configurations, which is found to be very similar to the gluon distribution measured in protons. The open question to the photon data is: is hadronic structure at low  $x$  universal, i.e., do the low- $x$  partons “know” about the partons in the high- $x$  region?

Measurements of the partonic structure of colour singlet exchange at HERA and the TEVATRON [19] for the first time show that such objects dominantly consist of gluons. Will these

measurements serve as a reference process for a gluon driven regime and offer new insight into QCD dynamics ?

Major contributions of lepton-hadron scattering in the past 10 years deepen our understanding of hadronic structures. Burning open questions ensure that this field of research will remain very active also in the coming decade.

## Acknowledgments

I wish to thank very much the Liverpool team for a wonderful conference ! For careful reading and comments to the manuscript I am grateful to E. Elsen and B. Foster. I wish to thank Th. Müller and the IEKP group of the University Karlsruhe for their hospitality, and the Deutsche Forschungsgemeinschaft for the Heisenberg Fellowship.

## References

- [1] H1 Collab., “Measurement of the Charged and Neutral Current Cross Sections at HERA”, contrib. paper 157b, International Europhysics Conference on High Energy Physics (HEP99), Tampere, Finland, 1999
- [2] ZEUS Collab., “Measurement of High  $Q^2$  Neutral, Charged Current Deep Inelastic Scattering Cross Sections in  $e^-p$  scattering at HERA”, contrib. papers 549, 558, International Europhysics Conference on High Energy Physics (HEP99), Tampere, Finland, 1999
- [3] H1 Collab., C. Adloff et al., *Eur. J. Phys. C* **13**, 609 (2000)
- [4] M. Erdmann, hep-ex/0007058, *Phys. Lett. B* **488**, 131 (2000)
- [5] ZEUS Collab., M. Derrick et al., *Z. Phys. C* **72**, 399 (1996)
- [6] BCDMS Collab., A.C. Benvenuti et al., *Phys. Lett. B* **223**, 485 (1989)
- [7] H1 Collab., S. Aid et al., *Nucl. Phys. B* **470**, 3 (1996)
- [8] M. Klein for the H1 Collab., hep-ex/0001059, Proc. XIX Int. Symp. on Lepton and Photon Interactions at High Energies, Stanford, USA (1999)
- [9] A. De Rujula et al., *Phys. Rev. D* **10**, 1649 (1974)
- [10] M. Glück, E. Reya, and A. Vogt, *Z. Phys. C* **53**, 127 (1992)
- [11] R.D. Ball and S. Forte, *Phys. Lett. B* **335**, 77 (1994)
- [12] Photon structure function data from review by R. Nisius, hep-ex/9912049, *Phys. Rept.* **332**, 165 (2000)
- [13] E. Witten, *Nucl. Phys. B* **120**, 189 (1977)

- [14] H1 Collab., C. Adloff et al., *Phys. Lett. B* **483**, 36 (2000)
- [15] H1 Collab., C. Adloff et al., *Z. Phys. C* **76**, 613 (1997)
- [16] M. Botje, hep-ph/9912439, *Eur. J. Phys. C* **14**, 285 (2000)
- [17] Workshop on the Nucleon Structure in High  $x$ -Bjorken Region, HiX2000, Temple University, Jefferson Lab, Philadelphia, USA (2000)
- [18] H1 Collab., C. Adloff et al., *Phys. Lett. B* **462**, 440 (1999)
- [19] CDF Collab., T. Affolder et al., *Phys. Rev. Lett.* **84**, 232 (2000)